EXIT-chart Aided Quantum Code Design Improves the Normalised Throughput of Realistic Quantum Devices

Hung Viet Nguyen, Zunaira Babar, Dimitrios Alanis, Panagiotis Botsinis, Daryus Chandra, Soon Xin Ng, and Lajos Hanzo

***Abstract*— In this contribution, the Hashing bound of Entanglement Assisted Quantum Channels (EAQC) is investigated in the context of quantum devices built from a range of popular materials, such as trapped ion and relying on solid state Nuclear Magnetic Resonance (NMR), which can be modelled as a so-called asymmetric channel. Then, Quantum Error Correction Codes (QECC) are designed based on Extrinsic Information Transfer (EXIT) charts for improving performance when employing these quantum devices. The results are also verified by simulations. Our QECC schemes are capable of operating close to the corresponding Hashing bound.**

I. Introduction

The appealing parallelism of quantum computing relying on quantum bits has inspired researchers to consider various quantum-related applications in the area of quantum communications [1]–[8]. However, a crucial obstacle to the practical realisation of quantum communications systems is the presence of quantum perturbations. Their deleterious effects can be mitigated by Quantum Error Correction Codes (QECCs). It was suggested that the employment of entanglement assistance is capable of further improving the performance of QECCs [9]–[11] in the context of the so-called symmetric depolarizing channel, which has been routinely used in theoretical studies. In the symmetric depolarizing channel characterised by the gross depolarizing probability p, each transmitted qubit may independently experience either a bit flip (X), a phase flip (Z), or both (Y) at a probability of $p_x = p_y = p_z = p/3$ [12]. By contrast, the materials considered at the time of writing for building quantum devices, including trapped ions [13] and solid state Nuclear Magnetic Resonance (NMR) [14], exhibit asymmetric depolarization property defined as the ratio of the phase flip probability over the bit flip probability, where the grade of asymmetry is in the range spanning from $\alpha = 10^2$ to $\alpha = 10^6$ [13]–[17]. QECCs designed for the asymmetric depolarizing channel were termed as asymmetric QECCs in [18]–[23], where a limited range of α values was assumed and no entanglement assistance was addressed. Hence, a more general framework covering both symmetric and asymmetric depolarizing channels is needed for Entanglement Assisted QECCs (EAQECCs).

To benchmark the design of the EAQECCs, the Entanglement Assisted Quantum Channel's (EAQC) capacity was investigated in [24], [25]. Accordingly, the so-called Hashing bound is advocated for setting a lower limit on the achievable quantum depolarizing channel capacity, which has been used for benchmarking the performance of various QECC schemes in [11], [12], [26]. Furthermore, the powerful Extrinsic Information Transfer (EXIT) chart technique [27]–[31] that was originally introduced for analysing the convergence behaviour of iterative decoding and detection in conventional communication systems was recently further developed for analysing the iterative decoding convergence of QECCs [12], [26]. Additionally, to the best of authors' knowledge contributions on entanglement assisted quantum coding schemes [11], [12], [26] and on the quantum depolarizing channel capacity [9], [24], [25], [32] only considered symmetric quantum depolarizing channels. Accordingly, the important milestones of the quantum channel's capacity (Hashing bound), EXIT charts, QECC as well as EAQECC are summarised in Fig. 1 along with the corresponding counterparts in the classical domain.

Against the above state-of-the-art, our novel contributions are as follows:

- *We provide an in-depth analysis of the entanglement-assisted quantum channel capacity from the perspective of realistic quantum devices, where the decoherence probability may be modelled by asymmetric quantum depolarizing channels. More explicitly, our analysis focuses on the conflicting code/channel attributes, namely on the quantum coding rate R_Q, on the channel's depolarizing probability p, on the channel's ratio of asymmetry α as well as on the entanglement consumption ratio E of the code.*
- *We demonstrate that the performance of iterative quantum codes invoked for asymmetric depolarizing channels can be accurately predicted by using the sophisticated EXIT-chart based method of [26].*
- *In contrast to the Quantum Irregular Convolutional Codes (QIrCC) of [12], which covers a limited portion of the EXIT chart, we conceive a QIrCC relying on Entanglement Assistance (QIrCCEA), which incorporates both unassisted as well as entanglement-assisted subcodes.*
- *We formulate an EXIT-chart based design procedure for*

The authors are with the School of Electronics and Computer Science, University of Southampton, Southampton, SO17 1BJ, UK (email: {hvn08r, zb2g10, da4g11, pb1y14, dc2n14, sxn, lh}@ecs.soton.ac.uk).

The financial support of the EPSRC under the grant EP/L018659/1, that of the European Research Council's, Advanced Fellow Grant and that of the Royal Society's Wolfson Research Merit Award is gratefully acknowledged. Additionally, the authors acknowledge the use of the IRIDIS High Performance Computing Facility, and associated support services at the University of Southampton, in the completion of this work.

This article has been accepted for publication in a future issue of this journal, but has not been fully edited. Content may change prior to final publication. Citation information: DOI 10.1109/ACCESS.2016.2591910, IEEE Access

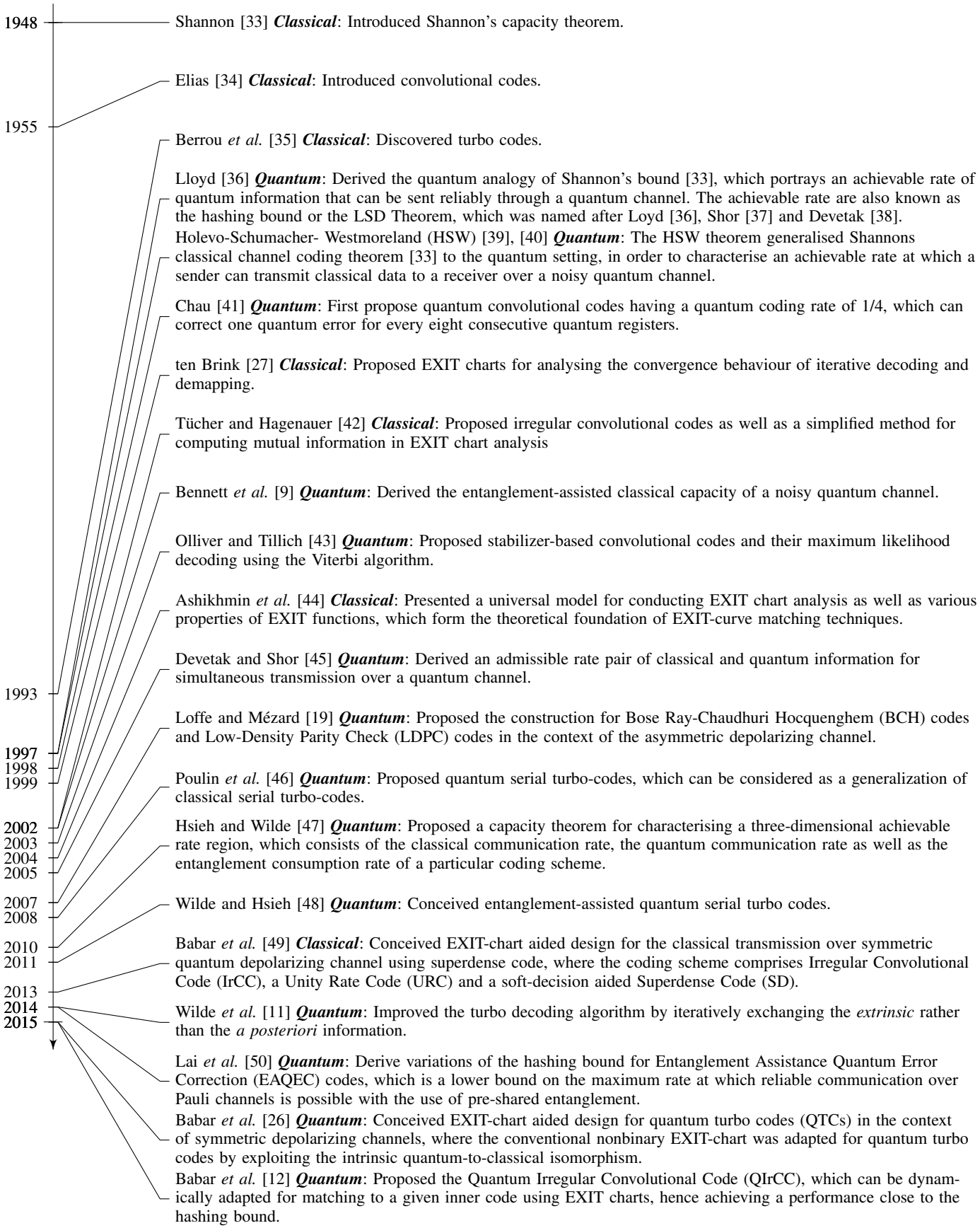

Fig. 1: Milestones along the road towards the EXIT-chart aided design of quantum codes used in realistic quantum devices.

demonstrating that the resultant EA-QIrCC is capable of approaching the Hashing bound in the EA-regime, which is considered in the context of asymmetric quantum depolarizing channels.

- *We demonstrate with the aid of a design example that our QIrCCEA provides an increased normalized throughput as well as an improved performance for realistic quantum channels, which are asymmetric in nature. In particular, our results demonstrate that the proposed QIrCCEA is capable of adapting its bit/phase flip error correcting capability according to the asymmetry of the channel model, thereby yielding the same residual Qubit Error Ratio (QBER) for X, Y as well as Z errors.*
- *We demonstrate that the coherence times associated with realistic quantum devices are substantially improved by the employment of our QIrCCEA coding scheme.*

The rest of this paper is organised according to Fig. 2 as follows. In Section II, a brief review of quantum depolarizing channels is provided for the sake of supporting the analyses of the EAQC capacity of Section III. Then, our code design and analysis using EXIT charts are presented in Section IV along with our discussions, before offering our conclusions in Section V.

II. Quantum Channel Model

A quantum depolarizing channel can be directly characterised by the specific materials employed for constructing quantum systems, including quantum gates. In other words, the quantum depolarizing channel can be used for modelling the imperfections in quantum hardware, namely qubit flips resulting from quantum decoherence and quantum gates. Furthermore, a quantum depolarizing channel can also model quantum-state flips imposed by the real transmission medium, including free-space wireless channels and optical fiber links, when qubits are transmitted across these media.The implementation of a quantum gate is prone both to decoherence and to systematic errors imposed by the quantum depolarizing channel, which ultimately results in an arbitrary error in the state of qubits, exemplified by a bit flip error (X), a phase flip error (Z) and by the joint occurrence of both a bit as well as a phase flip error (Y) [18]. Accordingly, quantum flip errors are characterised by the bit flip probability p_x as well as phase flip probability p_z and bit-and-phase flip probability p_y, which form a depolarizing channel, where the depolarizing probability of $p = p_x + p_z + p_y$ is considered as a gross error flip probability.

Most recent studies of the EAQC capacity [9], [24], [25], [32] as well as of QEC schemes considered the symmetric channel [10], [11], [26], where the constituent flip probabilities obey $p_x = p_y = p_z = p/3$. By contrast, popular materials invoked for producing quantum devices often exhibit asymmetric behaviour, where a phase flip is orders of magnitude more likely than a bit flip [19], which can be modelled by an asymmetric quantum depolarizing channel [13]–[17]. In such asymmetric channels, an extra parameter α termed as the channel's ratio of asymmetry is introduced for reflecting the ratio of the phase flip probability p_z and the bit flip probability p_x as [18], [51]

$$\alpha = \frac{p_z}{p_x} = 1 + 2\frac{e^{\frac{-t}{T_1}} - e^{\left(\frac{-t}{2T_1} - \frac{2t}{T_2}\right)}}{1 - e^{\frac{-t}{T_1}}}, \quad (1)$$

where T_1 is the relaxation time, while T_2 represents the dephasing time. The bit flip probability p_x as well as the simultaneous bit-and-phase flip probability p_y may be considered to be equal [18], [51]

$$p_y = p_x = \frac{1 - e^{\frac{-t}{T_1}}}{4}, \quad (2)$$

where t is the coherent operation duration of a physical quantum gate [52]. If the coherent operation duration t is relatively short, formulated as $t << T_1$, we can invoke the approximation of $\alpha \approx 2T_2/T_1 - 1$ [51]. As a result, the phase flip probability p_z can be directly determined from the values of α and p_x. Note that in the case of having $\alpha = 1$, the channel model represented by Eq. (1)-Eq. (2) becomes the symmetric channel model, where the condition of having $p_x = p_y = p_z = p/3$ is satisfied. In practice the channel's ratio of asymmetry has popular values of $\alpha = 10^2, 10^4, 10^6$ [13]–[17], for typical materials used for producing quantum devices, as listed in Table I.

System (Material)	T_1	T_2	α
P:Si [15]	1 hour	1ms	10^6
GaAs Quantum Dots [16]	10ms	$> 1\mu$s	10^4
Super conducting (flux qubits) [17]	1μs	100 ns	10^2
Trapped ions [13]	100 ms	1 ms	10^2
Solid State NMR [14]	> 1 min	> 1 s	10^2

TABLE I: Estimated asymmetric ratio α representing various quantum depolarizing channels associated with various quantum devices.

III. Formulation of Quantum Channel Capacity

A. Entanglement Assisted Capacity

Let us consider the entanglement assisted transmission scheme presented in Fig. 3, where B qubits of the source Alice are transmitted over a quantum depolarizing channel with the aid of entanglement assistance invoking B_S entangled qubits. It is assumed that the B_S entangled qubits are passed through an idealised noiseless quantum channel to Bob's receiver beforehand, for example during off-peak periods [11]. The process of transmitting the B qubits can be viewed as the Completely Positive Trace-Preserving (CPTP) mapping of [53] that maps a state ρ onto a linear combination of itself. For a gross depolarizing probability of p, the CPTP mapping may be represented by [51], [53]

$$N^{A\to B}(\rho) = (1 - p_x - p_y - p_z)\rho + p_x\mathbf{X}\rho\mathbf{X} + p_y\mathbf{Y}\rho\mathbf{Y} + p_z\mathbf{Z}\rho\mathbf{Z}\ , \quad (3)$$

where $\mathbf{X}$, $\mathbf{Y}$ and $\mathbf{Z}$ are Pauli errors [51] corresponding to the bit flip, the bit-and-phase flip and the phase flip, respectively. Let us focus our attention on the entanglement assisted Hashing bound that determines the specific code rate at which a certain

This article has been accepted for publication in a future issue of this journal, but has not been fully edited. Content may change prior to final publication. Citation information: DOI 10.1109/ACCESS.2016.2591910, IEEE Access

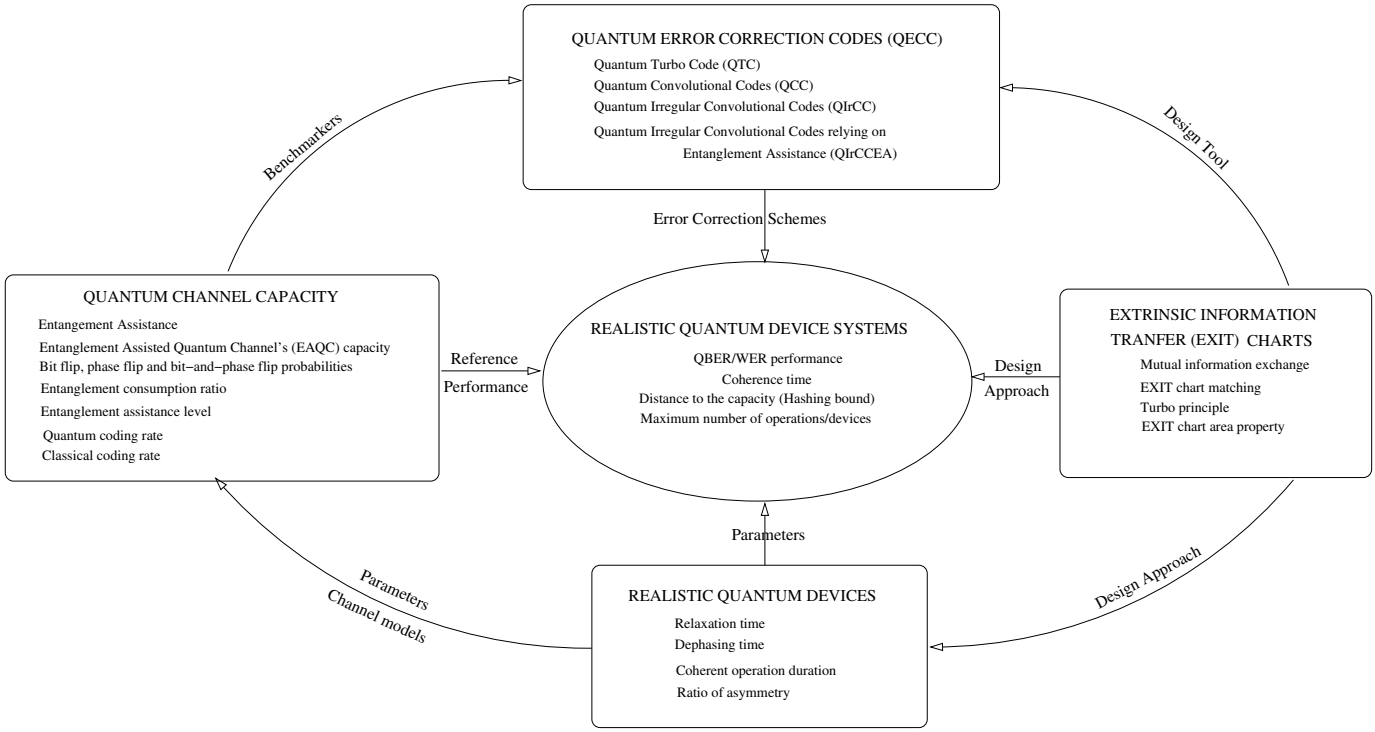

Fig. 2: Outline and rationale of the paper.

quantum code is capable of reliable operation for a particular depolarizing channel [9], [32]. The Hashing bound may be interpreted as the quantum depolarizing channel's capacity C_Q expressed as:

$$C_Q = 1 + (1-p)\log_2(1-p) + p_x \log_2(p_x) + p_y \log_2(p_y), + p_z \log_2(p_z). \quad (4)$$

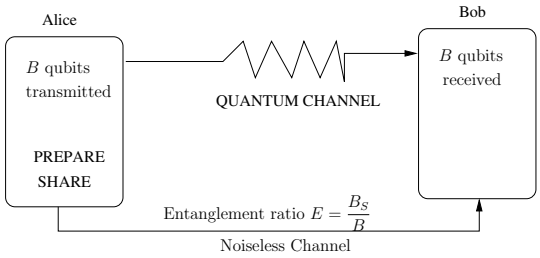

Fig. 3: Entanglement assisted transmission scheme

In the entanglement assisted system depicted in Fig. 3, both the source Alice and the destination Bob are allowed to access the B_S shared or entangled bits before communication commences [9]. Accordingly, the B_S entangled bits allow us to improve the performance of QECCs. Hence, the EAQC capacity C_Q^{EA} of the entanglement assisted system is higher than quantum depolarizing channel's capacity C_Q dispensing with the entanglement assistance [11], which is formulated as

$$C_Q^{EA} = C_Q + E, \quad (5)$$

where $E = \frac{B_S}{B}$ is the entanglement consumption ratio. For a quantum coding scheme having a quantum coding rate of R_Q, the maximum entanglement ratio is $E_{\max} = 1 - R_Q$ [12], [26]. Assuming that the system operates at its EAQC capacity when the maximal entanglement is applied, which implies that we have $R_Q = C_Q^{EA}|_{(E=E_{\max})}$, the maximum entanglement ratio $E_{\max}$ can be formulated from Eq. (5) as:

$$E_{\max} = \frac{1 - C_Q}{2}. \quad (6)$$

Hence, the EAQC capacity pertaining to the case of employing the maximal entanglement ratio may be written as:

$$C_Q^{EA}|_{(E=E_{\max})} = \frac{C_Q + 1}{2}. \quad (7)$$

In order to provide a holistic view of the EAQC capacity, which covers both entanglement assisted and entanglement unassisted systems, in Fig. 4 we characterise the EAQC capacity both as a function of the asymmetry ratio of $\alpha = (1 : 10^6)$ and of the depolarizing probability of $p = (0 : 1)$, where the entanglement assistance levels are $\theta = \frac{E}{E_{\max}} = \{0\%, 25\%, 75\%, 100\%\}$. Observe that the EAQC capacities presented in Fig. (5a)-(5d) grow sharply, when the level of asymmetry α increases from $\alpha = 1$ to $\alpha = 10^2$. However, only a marginal EAQC capacity improvement is exhibited when the level of asymmetry α increases further beyond $\alpha = 10^2$, as observed in Fig. 5b to Fig. 5d.

As seen in Fig. 4, the quantum depolarizing channel has a near-zero capacity upon approaching the point associated with $p = 0.5$ at an extremely high value of $\alpha = \frac{p_z}{p_x} = 10^6$. This is when the phase flip probability p_z becomes dominant, while both the bit flip probability p_x as well as the bit-and-phase flip probability p_y are equally negligible. In other words,

This article has been accepted for publication in a future issue of this journal, but has not been fully edited. Content may change prior to final publication. Citation information: DOI 10.1109/ACCESS.2016.2591910, IEEE Access

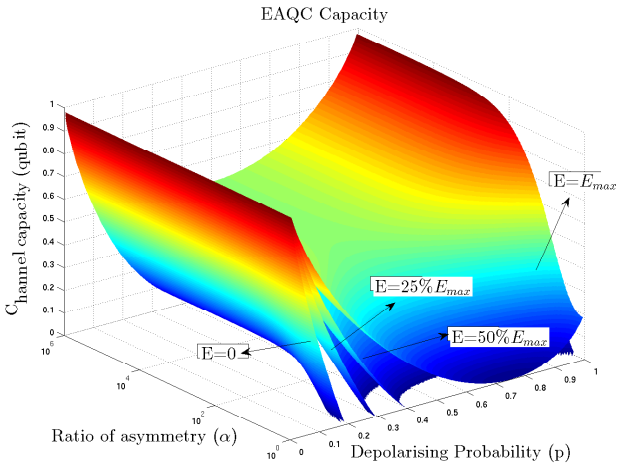

Fig. 4: EAQC capacity for different entanglement consumption ratios of $E = \theta E_{\max}$ associated with $\theta = \{0\%, 25\%, 75\%, 100\%\}$ versus ratio of asymmetry α and depolarizing probability p.

the perturbations caused by the quantum depolarizing channel solely depend on the phase flip probability p_z. As a result, the behaviour of the quantum depolarizing channel becomes similar to that of the Binary Symmetric Channel (BSC) in the high-α region.

As regards to the benefit of entanglement assistance, the EAQC capacity increases along with the entanglement consumption ratio E. This naturally raises further issues pertaining to the entanglement consumption ratio. For example, what is the optimal value and the maximum value of the entanglement ratio, when other constraints are imposed both on the coding rate as well as on the quantum depolarizing channel characteristics, namely on p and α.

Let us sample the EAQC capacity surfaces of Fig. 4 at particular values of $\alpha = \{1, 10^2, 10^4, 10^6\}$, in order to characterise the EAQC capacity in further detail. Accordingly, as seen from Fig. 5, the entanglement ratio at its maximum value E_{max} as given in Eq. (6) exhibits the highest channel capacity. For example, let us consider Fig. (5b), where the EAQC capacity associated with a quantum device having $\alpha = 10^2$ is characterised. We can see in Fig. (5b) that at the same gross quantum flip probability of $p = 0.3$, the maximum entanglement assistance $E = E_{max}$ provides a throughput improvement of $(0.53 - 0.07 = 0.46)$ qubits, which is equivalent to $0.53/0.07 \approx 780\%$ of the original throughput. A similar trend can be observed in Fig. (5c) and Fig. (5d) for quantum devices associated with $\alpha = 10^4$ and $\alpha = 10^6$, respectively. As seen in Fig. 5, the improvement of the EAQC capacity achieved by employing EA increases, as the gross flip probability p increases. Naturally, beyond its maximum, the advantage of the EAQC decreases, as the gross flip probability approaches $p = 1$. The maximum EAQC capacity improvement is achieved at a different value of p for a distinct α value, namely approximately at $p = \{0.75, 0.525, 0.50, 0.5\}$ for $\alpha = \{1, 10^2, 10^4, 10^6\}$, as seen in Fig. 5.

B. Different levels of entanglement

The maximal entanglement consumption ratio $E_{max} = 1 - R_Q$ can also be viewed as the 'optimal' entanglement ratio, which corresponds to the maximal achievable channel throughput [11], [12]. However, it is not practical to always employ the maximum entanglement ratio, because it would require all ancillary qubits to be replaced by entanglement qubits (ebits), each of which has a counterpart pre-shared. Hence, the EAQC capacity pertaining to various levels of entanglement ratios is also investigated here. Accordingly, the EAQC capacity of Eq. (5) may be also presented as

$$C_Q^{EA} = C_Q + \theta E_{\max}. \quad (8)$$

As a result, the EAQC capacity associated with different entanglement assistance levels, namely $\theta = \{10\%, 25\%, 50\%, 75\%\}$, are plotted in Fig. 5 for the various channels represented by the different values of α listed in Table I. It should be noted that when the entanglement assistance level θ is reduced, the EAQC capacity is also reduced, since reduced resources are invested in the entangled qubit transmission.

IV. Design and Analysis of Asymmetric QECC using EXIT Charts

In this section, we characterise the benefits of the EXIT-chart based method in two main aspects, namely in analysing a given coding scheme for a given channel and in designing a coding scheme for a specific channel. We first portray the general architecture of a quantum-domain concatenated coding scheme in Section IV-A for facilitating analyses on the benefits of the EXIT-chart based method. To conveniently describe the second beneficial aspect of designing QECCs according to Section IV-D, important traits of the QIrCCs relying on entanglement assistance are detailed in Section IV-C.

A. Entanglement Assisted QECC

To highlight the significance of different entanglement assistance levels (ratios), let us first consider a pair of coding schemes relying on two concatenated component codes, which have the general architecture portrayed in Fig. 6. Explicitly, both schemes have two component codes, namely the inner and the outer codes. In such coding schemes, information qubits are first encoded by the outer encoder for generating encoded qubits that are interleaved by the random interleaver π. Then, the interleaved qubits are encoded by the inner code before being transmitted over the quantum depolarizing channel. At the receiver side seen in Fig. 6, the outputs of the quantum channel are fed into the inverse encoder section in order to extract both the syndrome information and the corrupted information. Then, the syndrome information is fed into the iterative syndrome decoder section that takes in the inputs of the channel information and syndrome information in order to identify the associated error coset. Accordingly, the original information gleaned from the source is recovered at the sink by applying the error coset to the corrupted information within the recovery block R of Fig. 6.

This article has been accepted for publication in a future issue of this journal, but has not been fully edited. Content may change prior to final publication. Citation information: DOI 10.1109/ACCESS.2016.2591910, IEEE Access

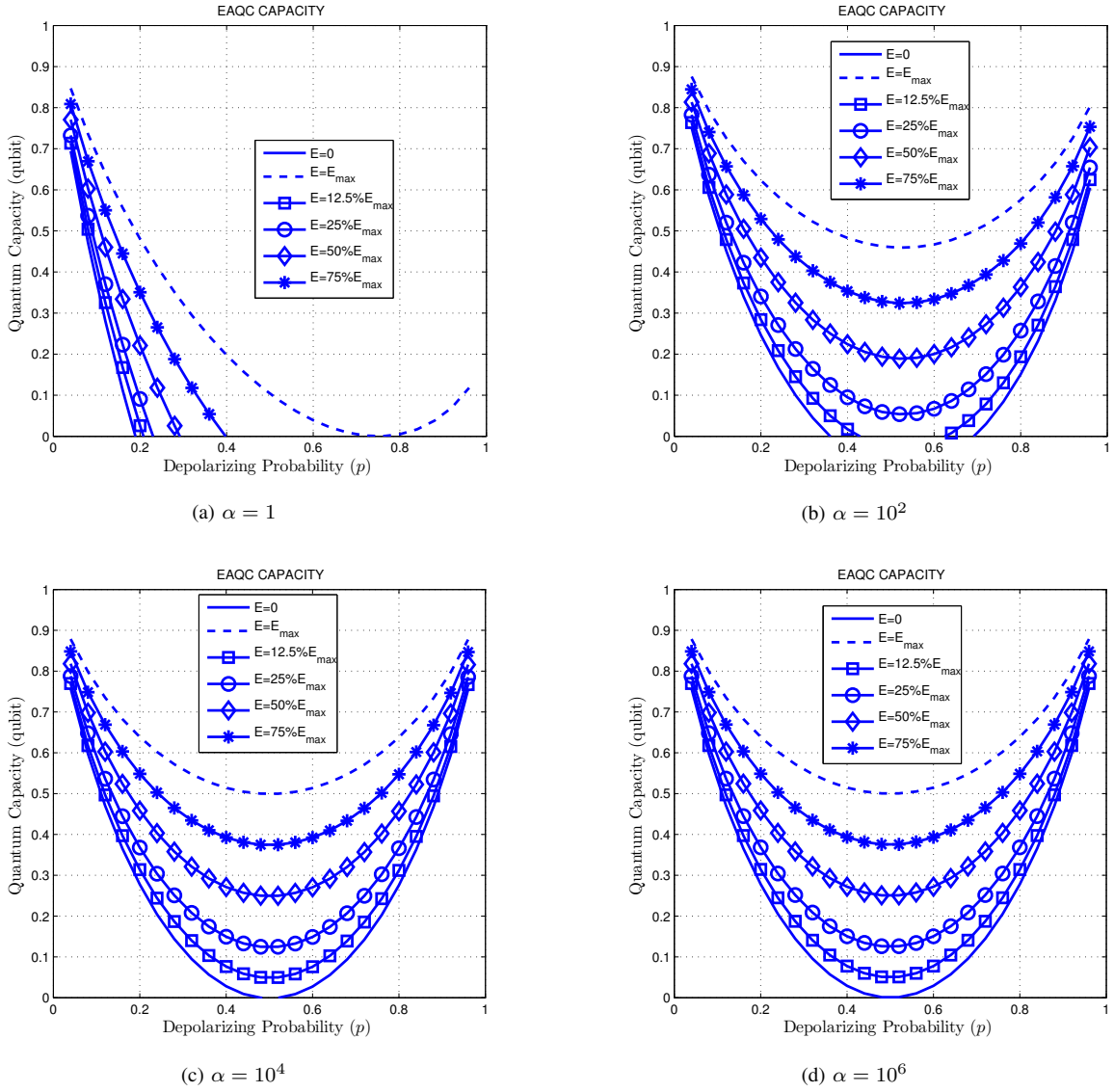

(a) $\alpha = 1$

(b) $\alpha = 10^2$

(c) $\alpha = 10^4$

(d) $\alpha = 10^6$

Fig. 5: The EAQC capacity versus the depolarizing probability parameterised by different entanglement assistance levels $\theta = \{0\%, 12.5\%, 25\%, 50\%, 70\%, 100\%\}$, when employing various quantum depolarizing channels characterised by the parameter α listed in Table I.

More specifically, the corrupted information word arriving from the output of the inner decoder is de-interleaved by π^{-1} within the inverse encoder section, before being decoded by the outer decoder for outputting the corrupted information. By contrast, the iterative syndrome decoder of Fig. 6 processes the syndrome extracted from both the inner and the outer decoder with the aid of the channel information. Accordingly, the inner syndrome decoder of Fig. 6 uses the channel information, the *a priori* information gleaned from the outer syndrome decoder (initialised to be equiprobable for the first iteration) and the inner syndrome for computing the extrinsic information, which is de-interleaved by the de-interleaver π^{-1} to create the input of the outer syndrome decoder of Fig. 6. The outputs of the outer syndrome decoder have two components, namely the *extrinsic* information and the *a posteriori* information, where the *extrinsic* information is used in the iteration for generating *a priori* information for the inner decoder with the aid of the interleaver π of Fig. 6. This iterative procedure continues until convergence to a vanishingly low $QBER$ is achieved or the maximum affordable number of iterations is reached. Finally, the *a posteriori* information of the outer decoder is used for determining the most likely error coset. It should be noted that both the inner and the outer code may invoke entanglement assistance with the aid of pre-shared qubits, as seen in Fig. 6.

1) PTO1R-PTO1R and PTO1REA-PTO1R schemes: The first scheme termed by the authors of [11] as PTO1R-outer/PTO1R-inner[1] is a non-entanglement assisted quantum

[1]The PTO1R component code termed based on the initials of the authors of [10], [46], who are D. Poulin, J-P. Tillich and H. Ollivier, as well as on the code identifier proposed in [10], [46].

This article has been accepted for publication in a future issue of this journal, but has not been fully edited. Content may change prior to final publication. Citation information: DOI 10.1109/ACCESS.2016.2591910, IEEE Access

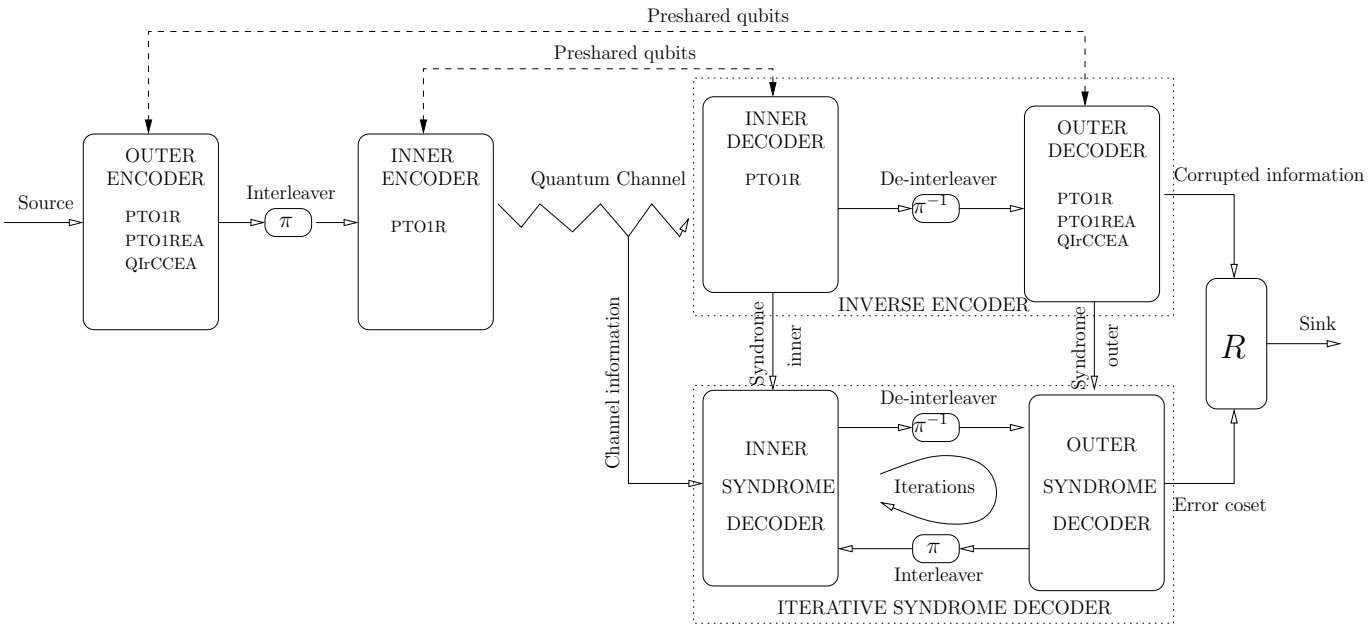

Fig. 6: General architecture of quantum concatenated coding schemes comprising two component codes invoking entanglement assistance.

coding scheme. This scheme was created from a similar code proposed in [10], [46], for comparison to the entanglement assisted coding scheme of [11] that was investigated in the context of symmetric quantum depolarizing channels. The second coding scheme is an entanglement assisted arrangement dubbed as PTO1REA-outer/PTO1R-inner in [11], where the term 'PTO1REA' represents the Entanglement Assisted (EA) version of the PTO1R code.

In the first coding scheme, namely in PTO1R-PTO1R, the inner and outer components are identical and they are based on the PTO1R code, which acts on three input memory qubits, one information qubit and two ancillary bits in order to generate three output memory qubits and three physical qubits. The construction of the component PTO1R code was random, which was configured to be comparable to the first code proposed in [10], where a seed transformation U was randomly generated. Then the state diagram detailed in [10] was used for testing, whether the corresponding encoder is catastrophic. A non-catastrophic and quasi-recursive code was selected as a benefit of their advantageous distance spectrum [11]. As a result, the decimal representation of the seed transformation associated with the PTO1R code is given by [11], [12]:

$$\begin{aligned} U &= 1355, 2847, 558, 2107, 3330, 739, \\ &\quad 2009, 286, 473, 1669, 1979, 189. \end{aligned}$$

Accordingly, the truncated distance spectrum polynomial of the PTO1R code is as follows [11]:

$$11x^5 + 47x^6 + 253x^7 + 1187x^8 + 6024x^9 + 30529x^{10}... \quad (9)$$

Note that the minimal distance represents the upper bound and cannot be directly related to the performance of the code. On one hand, the actual minimal distance of a turbo code depends on the interleaver, which was chosen randomly. On the other hand, the code is not decoded with the aid of a minimum distance decoder [10]. Hence, a large minimal distance does not necessarily imply having an excellent QBER/WER performance.

As for the second coding scheme of PTO1REA-PTO1R, the outer code PTO1REA is an entanglement assisted version of the inner code PTO1R, where again the seed transformation of Eq. (9) is used for the PTO1R encoder. More specifically, the outer code PTO1REA was formed by replacing the ancillary qubits by ebits, which activates the entanglement assistance for the PTO1REA codec of the PTO1REA-PTO1R coding scheme. The entanglement assistance manifests itself in terms of an improved distance spectrum polynomial [11] of

$$2x^9 + x^{10} + 5x^{11} + 8x^12 + 11x^{13} + 25x^{14}... \quad (10)$$

The inner code of these two schemes employs a code rate of $R_{in} = 1/3$ and the outer code is associated with a code rate of $R_{out} = 1/3$, hence the amalgamated code rate is $R_c = 1/9$. As a result, the corresponding maximum entanglement consumption rate becomes $E_{\max} = 1 - R_c = 8/9$. The value of the entanglement consumption ratio can be generally expressed as:

$$E = R_{in}\left(N_{out}^E R_{out} + N_{in}^E\right), \quad (11)$$

where N_{in}^E and N_{out}^E represent the number of entanglement qubits employed by the inner and outer codes, respectively.

B. Coding analysis employing EXIT charts

In order to analyse the performance of the quantum coding schemes presented in Fig. 8, we use the EXIT-chart based method of [49] recently proposed for analysing and designing quantum coding schemes for approaching the Hashing-bound [12], [26]. Accordingly, the ratio D of the quantum noise limit p^* calculated from the Hashing bound for the specific coding scheme and the equivalent gross flip probability p^E

estimated by the EXIT-chart based method for the specific coding scheme considered is used for quantifying, how close a code operates to the ultimate achievable limits [11], [12].

$$D = \frac{p^E}{p^*}. \quad (12)$$

It should be noted that the noise limit p^* may be determined by specifying a point on the capacity curves seen in Fig. 5 that corresponds to a given quantum coding rate R_Q.

Remark 1: The term noise limit in the context of quantum communication is defined in duality to the classical domain. More explicitly, for a given value of the gross flip probability p, $R_Q = C_Q^{EA}(p)$ of Eq. (5) represents the corresponding Hashing bound limit on the quantum coding rate. Conversely, for a given quantum coding rate R_Q leading to $R_Q = C_Q^{EA}(p^*)$, the value of p^* represents the corresponding Hashing limit on the depolarizing channel's gross flip probability [12].

It should be noted that a quantum depolarizing channel has properties similar to a BSC, but the extrinsic channel is an AWGN channel [54]. Additionally, for iterative decoding schemes the probability density functions of the extrinsic (*a priori*) values approach Gaussian distribution with increasing number of iterations. Therefore, two mains assumptions for EXIT charts are [54], [55]:

- the *a priori* values are fairly uncorrelated; and
- the probability density function of the *a priori* information has a Gaussian distribution.

The specific depolarizing probability p^E where a vanishingly low QBER is achieved will be estimated by EXIT chart analysis as follows. We first generate the EXIT curves of the PTO1R inner code for different values of the depolarizing probability, namely for $p = \{0.21, 0.22, 0.23, 0.24, 0.25\}$, as seen in Fig. 7 for the PTO1REA-PTO1R coding scheme. Then, the EXIT curves of the outer code PTO1REA are produced, followed by finding the highest value of the depolarizing probability that would still result in an open EXIT-chart tunnel. As a result, we can expect to see a vanishingly low QBER or Word Error Ratio (WER) in Fig. 8, for a depolarizing probability below to p^E. Accordingly, the ratio D of Eq. (12) between p^* and p^E is tabulated in Table II.

The staircase shaped Monte-Carlo simulation based decoding trajectory of the EXIT chart of Fig. 7 characterises the convergence behaviour of the coding scheme at a given depolarizing probability p and at a particular ratio of asymmetry α. For example, the trajectory plotted in Fig. 7 for $\alpha = 10^2$ and $p = 0.21$ suggests that for this asymmetric channel the decoder requires $I = 4$ iterations in order for its trajectory to reach the (1,1) point of the EXIT chart, which is associated with a vanishingly low QBER/WER. It can be inferred from Fig. 7 that using $I > 4$ iterations for the PTO1REA-PTO1R decoder may provide no further performance improvement at the depolarizing probability of $p = 0.21$. Naturally, the QBER-performance is degraded, when applying $I < 4$ iterations to the decoder. Hence, $I = 4$ represents the optimal number of iterations predicted by the EXIT chart of Fig. 7 for the PTO1REA-PTO1R scheme, where the decoder is capable of coping with a depolarizing probability of up to $p = 0.21$. These EXIT-chart based predictions are supported by the corresponding QBER-simulation results presented in Fig. 7.

Similarly, the above EXIT-chart based method is invoked for determining both the p^E value and the optimal number of iterations for both the entanglement assisted PTO1REA-PTO1R scheme and the unassisted PTO1R-PTO1R scheme, which operate upon different quantum devices associated with $\alpha = 1(\text{Sym}), 10^2, 10^4, 10^6$. Accordingly, all the corresponding performance curves plotted in Fig. 8 support our semi-analytical predictions of Table II obtained by the EXIT-chart based method. As a result, the ratio D is listed in Table II for each coding scheme invoked for a given quantum device pertaining to a single value of α.

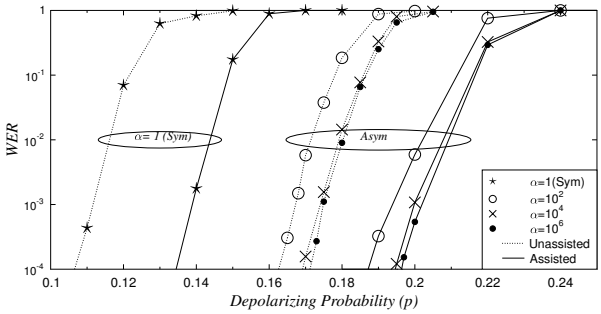

Fig. 8: WER versus depolarizing probability comparison of the PTO1REA-PTO1R and PTO1R-PTO1R schemes for both symmetric and asymmetric channels for an overall coding-rate of $R_Q = 1/9$ and an entanglement consumption ratio of $E = 1/9$, where the EXIT-chart based predictions and associated coding parameters are listed in Table II.

Additionally, the performance of the PTO1REA-PTO1R and PTO1R-PTO1R schemes is compared for the scenario of both symmetric and asymmetric quantum depolarizing channels in Fig. 8. The superiority of the entanglement assisted scheme observed in all the channels confirms the benefit of employing the entanglement regime. Moreover, by comparing the performance curves of Fig. 8 to the respective EAQC capacity curves of Fig. 5, we can see similarities in the relative positions between the performance curves of Fig. 8 and the corresponding capacity curves of Fig. 5, when the value of asymmetry ratio α changes from $\alpha = 1$ to $\alpha = 10^6$. This suggests that the EAQC capacity curves can be used for predicting the relative performance of coding schemes invoked for different quantum devices associated with diverse α values.

Moreover, it should be noted that a potentially error-free quantum channel exists for a throughput below the associated channel capacity. For example, observe in Fig. 8 that if the coding scheme PTO1REA-PTO1R having a coding rate of $R_Q = 1/9$ were used at the entanglement ratio of $E = 50\%E_{\max}$ leading to a better performance than that associated with $E = 25\%E_{\max}$ of Fig. 8, an error-free performance would be recorded. This is also confirmed by checking $R_Q = 1/9$ against the $E = 50\%E_{\max}$ scenario of Fig. (5b), where the corresponding Hashing bound has a minimum value higher than 0.2.

This article has been accepted for publication in a future issue of this journal, but has not been fully edited. Content may change prior to final publication. Citation information: DOI 10.1109/ACCESS.2016.2591910, IEEE Access

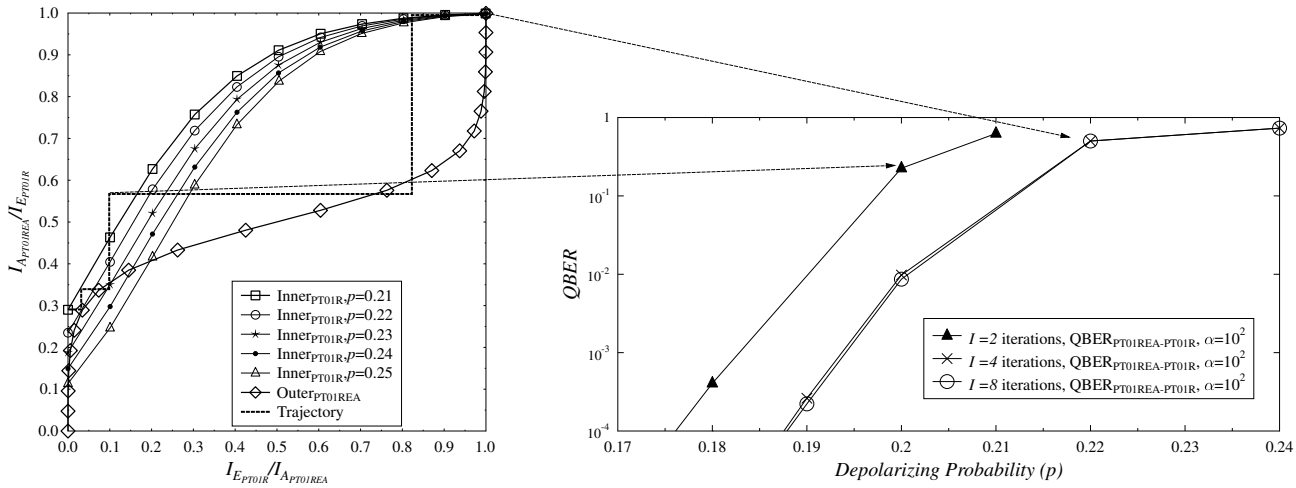

Fig. 7: EXIT chart analysis and associated QBER-performance of the PTO1REA-PTO1R coding scheme for the quantum device having the asymmetry ratio of $\alpha = 10^2$ at a depolarizing probability of $p = 0.21$, where the inner PTO1R and outer PTO1REA quantum code operating with the frame length of $L = 1000$ qubits have quantum coding rates of $R_{in} = 1/3$ and $R_{out} = 1/3$, yielding an overall quantum code rate of $R_Q = 1/9$. The entanglement qubits $N^E_{out} = 1$ of the outer PTO1REA code leads to the overall entanglement consumption ratio of $E = 1/8$, as calculated by Eq. (11) and detailed in Table II.

Entanglement ratio (E)	E=1/9=$E_{\max}/8, E_{\max} = 1 - R_Q = 8/9$			
Frame length (L)	L= 1000 qubits			
Overall quantum coding rate (R_Q)	$R_Q = R_{in} \times R_{out} = 1/3 \times 1/3 = 1/9$			
Asymmetric level (α)	1 (sym)	10^2	10^4	10^6
PTO1REA-PTO1R (Entanglement Assisted)				
Noise limit p^*	0.1758	0.3145	0.3655	0.3668
Value p^E	0.1600	0.2100	0.2400	0.2400
Optimised number of iterations I	4	4	4	4
Distance to capacity (D)	0.91	0.67	0.66	0.65
PTO1R-PTO1R(Unassisted)				
Noise limit p^*	0.1603	0.2729	0.3056	0.3064
Value p^E	0.1400	0.1950	0.2000	0.2000
Optimised number of iterations I	4	4	4	4
Distance to capacity (D)	0.87	0.71	0.65	0.65

TABLE II: Distance from vanishingly low QBER/WER region characterised by p^E estimated by the EXIT-chart based method for the PTO1REA-PTO1R and PTO1R-PTO1R schemes to the corresponding capacity point on Hashing bound a.k.a. the noise limit p^*.

C. Quantum Irregular Convolutional Codes with Entanglement Assistance

The QIrCC concept of [49] was proposed in the context of symmetric channels by invoking ideas from the classical domain, where Tüchler and Hagenauer [42], [56] proposed the employment of IrCCs for the design of near-capacity serial concatenated schemes, which are constituted by a family of convolutional codes (subcodes) having different rates. It must be noted that a QIrCC associated with Entanglement Assistance (QIrCCEA) relies on preshared qubits entangled between the encoder and decoder. These QIrCCs were specifically designed with the aid of EXIT charts for improving the convergence behaviour of iteratively decoded systems. Each quantum subcode ϕ encodes an appropriately selected fraction α_ϕ of the input qubit stream, where $\phi = [1, 2, ..., \Phi]$ and Φ is the number of subcodes. The appropriate fractions may be selected with the aid of EXIT-chart analysis in order to shape the inverted EXIT curve of the composite QIrCC for ensuring that its shape matches the EXIT curve of the inner decoder. Accordingly, an open EXIT-chart tunnel can be created even at high values of the depolarizing probability p, which implies approaching the quantum channel's capacity or the Hashing bound. Each subcode ϕ is characterised by its quantum code rate R^ϕ_Q as well as by the corresponding classical code rate R^ϕ_c and by the entanglement ratio E^ϕ, where the relationship between R^ϕ_Q and R^ϕ_c was presented in [12]. We have generalised the subcode ϕ for including entanglement assistance as follows:

$$R^\phi_c = \frac{1 + R^\phi_Q - E^\phi}{2}. \quad (13)$$

Naturally, the quantum subcode rate R_Q^ϕ always has to satisfy the following constraint

$$R_Q = \sum_{\phi=1}^{\Phi} \alpha_\phi R_Q^\phi \ , \tag{14}$$

$$E = \sum_{\phi=1}^{\Phi} \alpha_\phi E_Q^\phi \ , \tag{15}$$

where R_Q is the quantum coding rate (aggregate quantum coding rate) of the QIrCC, while E is the entanglement consumption ratio (aggregate entanglement consumption ratio) of the QIrCC.

D. Code design using EXIT charts

It is desirable to choose the QIrCCEA outer quantum code of Fig. 6 to be capable of performing well with an inner code associated with a diverse range of quantum coding rates as well as of supporting the entanglement assisted regime. As regards to the EXIT chart-based design, this means that the QIrCCEA outer quantum code has to have a composite EXIT curve having diverse convex as well as concave shapes for covering much of the EXIT chart area, so that it can match a wide range of inner decoder EXIT curves. As described by Eq. (14) and Eq. (15), the composite EXIT curve of the QIrCC is formed by combining the appropriately weighted EXIT curves associated with the subcodes of our choice. For example, the QIrCC constructed from the subcodes having the EXIT curves plotted in Fig. 9a is capable of providing a better EXIT curve matching than that constructed from the subcodes pertaining to the EXIT curves plotted in Fig. 9b, when the inner decoder's EXIT curve is within the lower part of the EXIT chart.

As a result, we first conceive a QIrCCEA outer code by incorporating both unassisted as well as entanglement assisted subcodes. Then, to explicitly demonstrate the benefits of EXIT charts in designing asymmetric QECCs, we present the design of the quantum-domain concatenated coding scheme portrayed in Section IV-A. The outer code QIrCCEA characterised in Section IV-C is considered. Note that we use the same PTO1R inner code in order to contrast to the PTO1REA-PTO1R scheme analysed in Section 7. For the sake of readability, we present this section in the form of design guidelines including two phases containing a number of steps, in which our design examples are used for the sake of illustration.

In the **first phase**, we conceive a beneficial set of subcodes in order to construct a QIrCCEA code whose composite EXIT curve is capable of tuning its shape for covering a wide area of EXIT chart as well as of supporting various entanglement consumption ratios. These beneficial capabilities may allow the resultant QIrCCEA code to perform well, when concatenated according to Fig. 6 with the inner code PTO1R in the context of the specific asymmetric depolarizing channel considered. Accordingly, subcodes generated from a mother-code [57] are retained/discarded based upon the following criteria:

- Have a diverse range of the quantum coding rate;
- Have a diverse range of entanglement ratio;
- Pass the non-catastrophic criterion test of [10];
- Have an EXIT curve satisfying the EXIT-chart's area property [58], where the area under the EXIT curve is proportional to the classical coding rate of Eq. (13).

Remark 2: *The area under the EXIT curve of an inner decoder component is approximately equal to the attainable channel capacity, provided that the channel's input symbols are equiprobable* [44], [59]. This property [44], [59] may be exploited for determining the achievable rates of forward error control schemes relying on iterative multi-stage coding. Then, the achievable capacity may be used for selecting a specific coding scheme from the available set and may also be used for optimising coding arrangements relying on numerous parameters by using the achievable capacity as a criterion for comparing all legitimate sets of parameters used for specifying the coding arrangement.

As a result, the resultant set of meritorious subcodes is listed in Table III, while the corresponding EXIT curves are plotted in Fig. 9a, where the labels 'assisted' and 'unassisted' represents the entanglement-assisted subcode and the subcode dispensing with entanglement assistance, respectively. In Table III, each subcode is characterised by its quantum code rate R_Q as well as by the corresponding classical code rate R_c and the entanglement ratio E.

The **second phase** is dedicated to the near-capacity design carried out according to the specific design requirements, which may proceed as follows:

- Optimise the inner code by finding the most appropriate coding configuration for the given channel conditions. In our design example, we use the PTO1R code for the sake of a fair comparison to the previous work [11], [12], [26], [49] investigated in the context of the symmetric quantum depolarizing channel.
- Create the EXIT curve of the inner PTO1R decoder using the method detailed in [49] for different depolarizing probabilities, namely for $p = 0.26, 0.30, 0.35$, as seen in Fig. 12.
- Use the subcode set of Table III and then invoke the EXIT curve matching algorithm of [42] for generating the optimised weighting coefficients α_ϕ associated with the highest possible value of depolarizing probabilities p, provided that a sufficiently wide open EXIT tunnel may be seen. Note that the resultant optimised weighting coefficients α_ϕ listed in Fig. 12 have to satisfy both Eq. (14) and Eq. (15).
- The optimised weighting coefficients seen in Fig. 12 are used in the QIrCCEA codec in order to generate the staircase-shaped decoding trajectory plotted in Fig. 12, where the most appropriate number of iterations is determined by counting the number of steps, yielding $I = 8$.

Remark 3: It should be noted that we need to have a great number of subcodes in order to always find out a set of optimised weighting coefficients satisfying both Eq. (14) and Eq. (15), when arbitrary values of target R_Q and E are given. In our example of employing $\Phi = 13$ subcodes, the resulting set of optimised weighting coefficients detailed in Fig. 12

This article has been accepted for publication in a future issue of this journal, but has not been fully edited. Content may change prior to final publication. Citation information: DOI 10.1109/ACCESS.2016.2591910, IEEE Access

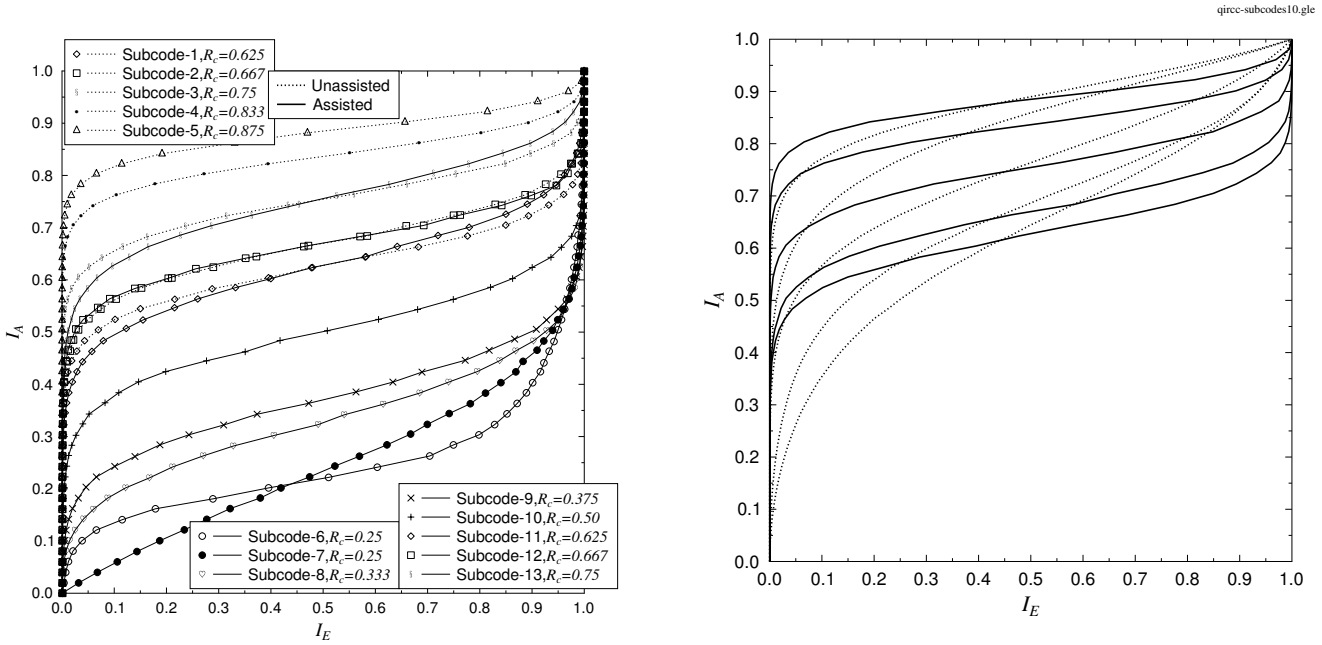

(a) EXIT curves of the proposed subcodes listed in Table III and used for constructing our QIrCCEA.

(b) EXIT curves of the subcodes used for forming the QIrCC presented in [12]

Fig. 9: EXIT curves of the subcodes listed in Table III in comparison to those of the subcodes presented in [12].

Subcode	Subcode Configurations
1	$[R_Q^1, R_c^1, E^1] = [0.25, 0.625, 0]$; $U_1 = [9600, 691, 11713, 4863, 1013, 6907, 1125, 828, 10372, 6337, 5590, 11024, 12339, 3439]$
2	$[R_Q^2, R_c^2, E^2] = [0.33, 0.667, 0]$; $U_2 = [3968, 1463, 2596, 3451, 1134, 3474, 657, 686, 3113, 1866, 2608, 2570]$
3	$[R_Q^3, R_c^3, E^3] = [0.5, 0.75, 0]$; $U_3 = [848, 1000, 930, 278, 611, 263, 744, 260, 356, 880]$
4	$[R_Q^4, R_c^4, E^4] = [0.667, 0.833, 0]$; $U_4 = [529, 807, 253, 1950, 3979, 2794, 956, 1892, 3359, 2127, 3812, 1580]$
5	$[R_Q^5, R_c^5, E^5] = [0.75, 0.875, 0]$; $U_5 = [62, 6173, 4409, 12688, 7654, 10804, 1763, 15590, 6304, 3120, 2349, 1470, 9063, 4020]$
6	$[R_Q^6, R_c^6, E^6] = [0.25, 0.25, 0.75]$; $U_6 = [4805, 14753, 6723, 7140, 3037, 8204, 3405, 11119, 2358, 7526, 9564, 404, 3354, 8611]$
7	$[R_Q^7, R_c^7, E^7] = [0.25, 0.25, 0.75]$; $U_7 = [573, 3574, 789, 2119, 1048, 862, 2839, 427, 2933, 2276, 443, 540]$
8	$[R_Q^8, R_c^8, E^8] = [0.25, 0.333, 0.667]$; $U_8 = [981, 766, 4012, 3708, 2416, 2168, 1210, 2515, 2892, 1781, 2776, 2843]$
9	$[R_Q^9, R_c^9, E^9] = [0.25, 0.375, 0.5]$; $U_9 = [14704, 11303, 7079, 9128, 8516, 3097, 5487, 11095, 15857, 6765, 608, 465, 5956, 8172]$
10	$[R_Q^{10}, R_c^{10}, E^{10}] = [0.5, 0.50, 0.5]$; $U_{10} = [5596, 15439, 5141, 486, 2473, 7611, 16073, 1681, 13709, 2967, 1829, 14551, 3430, 43]$
11	$[R_Q^{11}, R_c^{11}, E^{11}] = [0.5, 0.625, 0.25]$; $U_{11} = [4429, 9095, 11436, 2362, 2843, 694, 10361, 13034, 14132, 2913, 9921, 9627, 12088, 9777]$
12	$[R_Q^{12}, R_c^{12}, E^{12}] = [0.667, 0.667, 0.333]$; $U_{12} = [838, 1616, 3675, 2328, 604, 2652, 3728, 1118, 540, 3272, 365, 3830]$
13	$[R_Q^{13}, R_c^{13}, E^{13}] = [0.7, 0.75, 0.5]$; $U_{13} = [15317, 456, 6176, 3385, 15391, 7198, 527, 316, 8508, 9499, 13081, 3004, 15507, 12318]$

TABLE III: List of subcodes detailing their quantum coding rate R_Q^ϕ, classical coding rate R_c^ϕ, entanglement ratio E^ϕ as well as the decimal representation U_ϕ of the seed transformation, where we have the number of subcode $\phi = \{1, ..., 13\}$.

This article has been accepted for publication in a future issue of this journal, but has not been fully edited. Content may change prior to final publication. Citation information: DOI 10.1109/ACCESS.2016.2591910, IEEE Access

corresponds to the outer QIrCCEA coding rate $R_Q = 0.66$ and the outer QIrCCEA entanglement ratio of $E = 0.19$.

Accordingly, we arrive at the EXIT chart presented in Fig. 12, where again $I = 8$ iterations are sufficient at a depolarizing probability of $p^E = 0.26$ for the QIrCCEA-PTO1R scheme to perform close to the Hashing bound represented by the corresponding noise limit of $p^* = 0.3118$, as seen in Table IV. The EXIT-chart based predection is confirmed by our QBER/WER simulation results presented in Fig. 10. More specifically, the QBER-performance of the QIrCCEA-PTO1R scheme is substantially improved upon increasing the number of iterations from $I = 2$ to $I = 8$. By contrast, applying $I > 8$ iterations to the QIrCCEA-PT01R provides no significant QBER-performance improvement as seen in Fig. 12, hence confirming that $I = 8$ is the most appropriate number of iterations.

As a result of the improved EXIT curve matching seen in Fig. 12 in comparison to that of Fig. 7, a significant WER performance improvement can be obtained upon employing the QIrCCEA instead of the PTO1REA, as observed in Fig. 10, which corresponds to a ratio of $D = 0.83$ w.r.t. the associated noise limit. Furthermore, apart from an improved WER performance, our QIrCCEA-PTO1R scheme has a higher quantum coding rate of $R_Q = 0.21$ than the rate of $R_Q = 0.11$ used for the PTO1REA-PTO1R scheme.

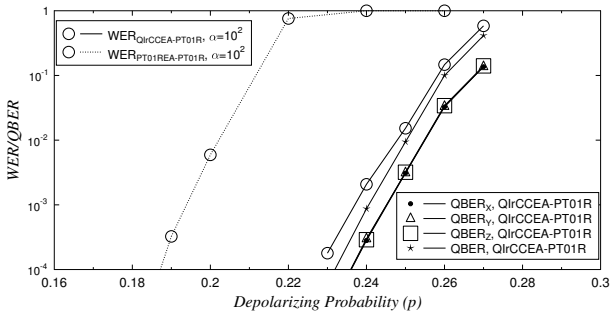

Fig. 10: WER/QBER versus depolarizing probability comparison of the QIrCCEA-PTO1R and PTO1REA-PTO1R schemes using a frame length $L = 1000$ qubits at the channel asymmetry ratio of $\alpha = 100$, where the parameters of the two coding schemes are comparatively detailed in Table IV.

Additionally, despite the fact that the phase flip probability p_z is $\alpha = 10^2$ times higher than the bit flip probability p_x as well as the bit-and-phase flip probability p_y, in Fig. 10 we observe similar values of $QBER_x, QBER_y, QBER_z$ for the three type of errors, namely for the bit, bit-and-phase as well as for the phase errors. As an important conclusion, our QIrCCEA-PTO1R scheme is capable of equalising the influence of these three quantum error types. This benefit of our QIrCCEA-PTO1R scheme is directly reflected by the improvement of the so-called effective relaxation time T_{1e} and effective dephasing time T_{2e}, which are also termed as effective coherence times. The effective times are defined by Eq. (1) and Eq. (2), where the bit-flip and phase-flip probabilities are substituted by the $QBER_x$ and $QBER_z$, respectively, while the coherent operation duration t of a physical quantum gate remains unchanged. Accordingly, the coherence time improvement is plotted in Fig. 11 for the trapped ion based devices of Table I, where we have $T_1 = 100$ ms and $T_1 = 1$ ms at a channel asymmetry ratio of $\alpha = 100$. As seen in Fig. 11, both the relaxation time T_1 and the dephasing time T_2 have been significantly increased in the target operating region seen in Fig. 10 for the QIrCCEA-PTO1R coding scheme, where we have $QBER < 10^2$. The highest effective dephasing time of $T_{2e} \approx 10^4$ ms is about 10000 times higher than the original dephasing time of $T_1 = 1$ ms as well as the adequate operation duration of $t \approx 1$ ms. Hence, in practice the employment of the QIrCCEA-PTO1R coding scheme may allow us to bundle significantly more gate operations into the effective dephasing time.

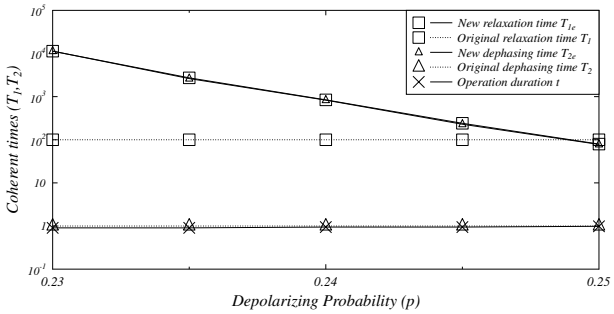

Fig. 11: Improvement in coherent times, namely of relaxation time T_1 and dephasing time T_2, for Trapped ions based devices of Table I, when employing the QIrCCEA-PTO1R coding scheme using a frame length $L = 1000$ qubits at the channel asymmetry ratio of $\alpha = 100$.

V. Conclusions

In this contribution, we have analysed the EAQC capacity curves and conceived design guidelines for quantum coding schemes that are capable of eliminating the deleterious effects of quantum flips in quantum devices. Our EXIT chart based technique was demonstrated to be a useful tool for both analysing and designing quantum coding schemes. Our simulation results support our semi-analytical results. The results may be readily used for designing QECC schemes in order to mitigate the errors introduced by quantum devices built from various materials, including trapped ions and solid state Nuclear Magnetic Resonance, which are investigated by the quantum hardware community.

References

[1] L. Ma, A. Mink, H. Xu, O. Slattery, and X. Tang, "Experimental demonstration of an active quantum key distribution network with over GBPS clock synchronization," *IEEE Communications Letters*, vol. 11, pp. 1019–1021, December 2007.

[2] L. Ma, T. Chang, A. Mink, O. Slattery, B. Hershman, and X. Tang, "Experimental demonstration of a detection-time-bin-shift polarization encoding quantum key distribution system," *IEEE Communications Letters*, vol. 12, pp. 459–461, June 2008.

[3] I. Djordjevic, "Quantum LDPC Codes from Balanced Incomplete Block Designs," *IEEE Communications Letters*, vol. 12, pp. 389–391, May 2008.

[4] J. Li, X.-B. Chen, G. Xu, Y.-X. Yang, and Z.-P. Li, "Perfect quantum network coding independent of classical network solutions," *IEEE Communications Letters*, vol. 19, pp. 115–118, Feb 2015.

	Coding Schemes	
Parameters	**QIrCCEA-PTO1R**	**PTO1REA-PTO1R**
Inner codes (R_{in}, N_{in}^{E})	PTO1R (1/3,0)	PTO1R (1/3,0)
Outer code rate R_{out}	0.49 (from Eq. (14))	0.33
Outer code entanglement ratio E_{out}	0.29 (from Eq. (15))	0.33
Noise limit p^* from Eq. (8)	0.3118	0.3145
p^E predicted by the EXIT chart method	0.26	0.21
Code rate $R_Q = R_{in} * R_{out}$	0.16	0.11

TABLE IV: Comparative parameters of the QIrCCEA-PTO1R and PTO1REA-PTO1R coding schemes.

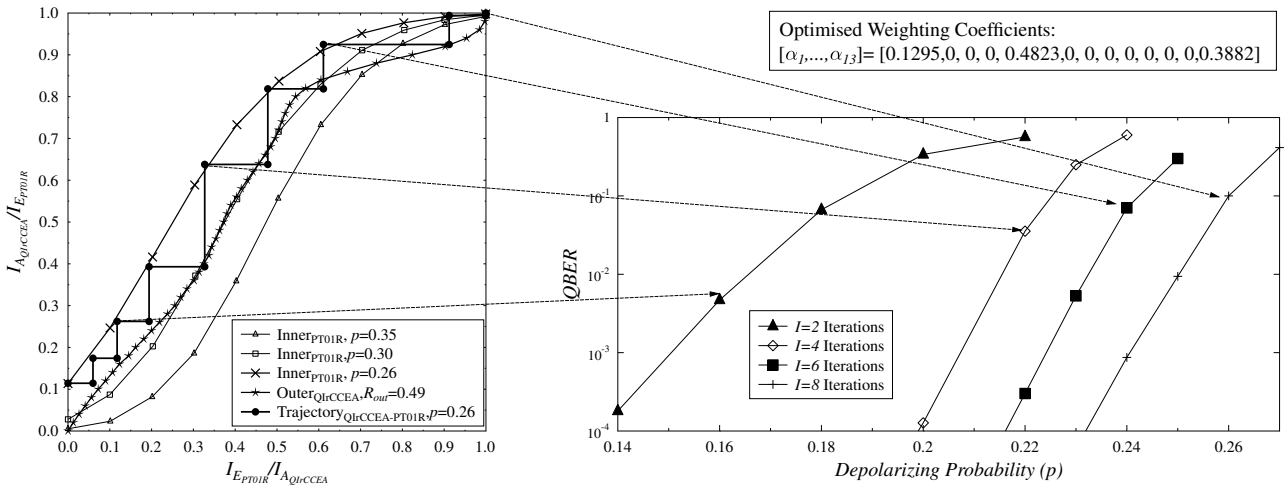

Fig. 12: EXIT chart and associated QBER-performance of the QIrCCEA-PTO1R coding scheme using the inner PTO1R code ($R_{in} = 0.33$) and the outer QIrCCEA code ($R_{out} = 0.49$), having the overall quantum code rate of $R_Q = R_{in}R_{out} = 0.16$.

	LIST of ACRONYMS
BSC	Binary Symmetric Channel
CPTP	Completely Positive Trace-Preserving
EA	Entanglement Assisted
EAQC	Entanglement Assisted Quantum Channels
EAQECC	Entanglement Assisted Quantum Error Correction Code
ebits	Entanglement qubit
EXIT	Extrinsic Information Transfer
NMR	Nuclear Magnetic Resonance
QBER	Qubit Error Ratio
QECC	Quantum Error Correction Code
QIrCC	Quantum Irregular Convolutional Code
QIrCCEA	Quantum Irregular Convolutional Code relying on Entanglement Assistance
WER	Word Error Ratio

[5] T. Shang, X.-J. Zhao, and J.-W. Liu, "Quantum network coding based on controlled teleportation," *IEEE Communications Letters*, vol. 18, pp. 865–868, May 2014.

[6] J. Kelly, R. Barends, A. G. Fowler, A. Megrant, E. Jeffrey, T. C. White, D. Sank, J. Y. Mutus, B. Campbell, Yu Chen, Z. Chen, B. Chiaro, A. Dunsworth, I.-C. Hoi, C. Neill, P. J. J. O'Malley, C. Quintana, P. Roushan, A. Vainsencher, J. Wenner, A. N. Cleland, John M. Martinis, "State preservation by repetitive error detection in a superconducting quantum circuit," *Nature*, vol. 519, pp. 66–69, Mar. 5 2015.

[7] G. D. Paparo and M. A. Martin-Delgado, "Google in a quantum network," *Scientific Report*, vol. 2, Jun. 8 2012.

[8] Schindler et al., "A quantum information processor with trapped ions," *New Journal of Physics*, vol. 15, Dec. 6 2013.

[9] C. Bennett, P. Shor, J. Smolin, and A. Thapliyal, "Entanglement-assisted capacity of a quantum channel and the reverse Shannon theorem," *IEEE Transactions on Information Theory*, vol. 48, pp. 2637–2655, Oct 2002.

[10] D. Poulin, J. Tillich, and H. Ollivier, "Quantum serial turbo codes," *IEEE Transactions on Information Theory*, vol. 55, pp. 2776–2798, June 2009.

[11] M. Wilde, M.-H. Hsieh, and Z. Babar, "Entanglement-assisted quantum turbo codes," *IEEE Transactions on Information Theory*, vol. 60, pp. 1203–1222, Feb 2014.

[12] Z. Babar, P. Botsinis, D. Alanis, S. X. Ng, and L. Hanzo, "The road from classical to quantum codes: A hashing bound approaching design procedure," *IEEE Access*, vol. 3, pp. 146–176, 2015.

[13] F. Schmidt-Kaler, S. Gulde, M. Riebe, T. Deuschle, A. Kreuter, G. Lancaster, C. Becher, J. Eschner, H. Hffner, and R. Blatt, "The coherence of qubits based on single Ca+ ions," *Journal of Physics B-Atomic Molecular and Optical Physics*, vol. 36, pp. 623–636, Feb. 14 2003.

[14] L. Vandersypen, M. Steffen, G. Breyta, C. Yannoni, M. Sherwood, and I. Chuang, "Experimental realization of Shor's quantum factoring algorithm using nuclear magnetic resonance," *Nature*, vol. 414, pp. 883–887, Dec. 20 2001.

[15] A. M. Tyryshkin, J. J. L. Morton, S. C. Benjamin, A. Ardavan, G. A. D. Briggs, J. W. Ager, and S. A. Lyon, "Coherence of spin qubits in silicon," *Journal of Physics-Condensed Matter*, vol. 18, pp. S783–S794, May 31 2006.

[16] J. R. Petta, A. C. Johnson, J. M. Taylor, E. A. Laird, A. Yacoby, M. D. Lukin, C. M. Marcus, M. P. Hanson, and A. C. Gossard, "Coherent manipulation of coupled electron spins in semiconductor quantum dots," *SCIENCE*, vol. 309, pp. 2180–2184, Sep. 30 2005.

[17] P. Bertet, I. Chiorescu, G. Burkard, K. Semba, C. J. P. M. Harmans, D. P. DiVincenzo, and J. E. Mooij, "Dephasing of a superconducting qubit induced by photon noise," *Physical Review Lettes*, vol. 95, Dec. 16 2005.

	LIST of SYMBOLS
α_ϕ	Coding fraction of subcode ϕ
α	Channel's ratio of asymmetry
θ	Entanglement level
B_S	Number of Entangled Qubits
B	Number of Transmitted Qubits
C_Q^{EA}	Quantum depolarizing channel's capacity with entanglement assistance
C_Q	Quantum depolarizing channel's capacity
D	A ratio to quantify how close a code operates to the ultimate achievable limits
E^ϕ	Entanglement consumption ratio of subcode ϕ
$E_{\max}$	Maximum entanglement consumption ratio
E	Entanglement consumption ratio
I	Number of iterations
N_{in}^E	Number of entangled qubits at the inner code
N_{out}^E	Number of entangled qubits at the outer code
p^*	Corresponding Hashing limit on the depolarizing channel's gross flip probability
p^E	Equivalent gross flip probability p^E estimated by the EXIT-chart based method
p_x	Bit flip probability
p_y	Bit and phase flip probability
p_z	Phase flip probability
p	Gross flip probability or channel's depolarizing probability
$QBER_x$	Qubit error ratio corresponding to bit flip errors
$QBER_y$	Qubit error ratio corresponding to bit-and-phase flip errors
$QBER_z$	Qubit error ratio corresponding to phase flip errors
R_c^ϕ	Quantum coding rate of subcode ϕ
R_Q^ϕ	Classical coding rate of subcode ϕ
R_{in}	Quantum coding rate of the inner code
R_{out}	Quantum coding rate of the outer code
R_Q	Quantum coding rate
T_{1e}	Effective relaxation time
T_{2e}	Effective dephasing time
T_1	Relaxation time
T_2	Dephasing time
t	Coherent operation duration
U_ϕ	Decimal representation of the seed transformation associated with subcode ϕ
U	Decimal representation of the seed transformation
$\mathbf{X}$	Bit flip
$\mathbf{Y}$	Bit-and-phase flip
$\mathbf{Z}$	Phase flip

[18] Z. W. E. Evans, A. M. Stephens, J. H. Cole, L. C. L. Hollenberg, "Error correction optimisation in the presence of X/Z asymmetry," *ArXiv*, 2007.

[19] L. Loffe, and M. Mezard, "Asymmetric quantum error-correcting codes," *Physical Review A*, vol. 75, no. 3, p. 032345, 2007. PRA.

[20] L. Wang, K. Feng, S. Ling, and C. Xing, "Asymmetric quantum codes: Characterization and constructions," *IEEE Transactions on Information Theory*, vol. 56, pp. 2938–2945, June 2010.

[21] M. Ezerman, S. Ling, and P. Sole, "Additive asymmetric quantum codes," *IEEE Transactions on Information Theory*, vol. 57, pp. 5536–5550, Aug 2011.

[22] M. Ezerman, S. Jitman, S. Ling, and D. Pasechnik, "CSS-like constructions of asymmetric quantum codes," *IEEE Transactions on Information Theory*, vol. 59, pp. 6732–6754, Oct 2013.

[23] G. La Guardia, "On the construction of asymmetric quantum codes," *International Journal of Theoretical Physics*, vol. 53, no. 7, pp. 2312–2322, 2014.

[24] K. Bradler, P. Hayden, D. Touchette, and M. Wilde, "Trade-off capacities of the quantum Hadamard channels," *Physical Review A*, vol. 81, Jun. 14 2010.

[25] M. Wilde and M.-H. Hsieh, "The quantum dynamic capacity formula of a quantum channel," *Quantum Information Processing*, vol. 11, pp. 1431–1463, Dec. 2012.

[26] Z. Babar, S. X. Ng, and L. Hanzo, "Exit-chart-aided near-capacity quantum turbo code design," *IEEE Transactions on Vehicular Technology*, vol. 64, pp. 866–875, March 2015.

[27] S. ten Brink, "Convergence of iterative decoding," *Electronics Letters*, vol. 35, pp. 806–808, May 13, 1999.

[28] S. ten Brink and G. Kramer, "Design of repeat-accumulate codes for iterative detection and decoding," *IEEE Transactions on Signal Processing*, vol. 51, pp. 2764–2772, Nov 2003.

[29] S.-J. Lee, A. Singer, and N. Shanbhag, "Linear turbo equalization analysis via BER transfer and EXIT charts," *IEEE Transactions on Signal Processing*, vol. 53, pp. 2883–2897, Aug 2005.

[30] J. Karjalainen, M. Codreanu, A. Tolli, M. Juntti, and T. Matsumoto, "EXIT chart-based power allocation for iterative frequency domain MIMO detector," *IEEE Transactions on Signal Processing*, vol. 59, pp. 1624–1641, April 2011.

[31] F. Babich, A. Crismani, M. Driusso, and L. Hanzo, "Design criteria and genetic algorithm aided optimization of three-stage-concatenated space-time shift keying systems," *Signal Processing Letters, IEEE*, vol. 19, pp. 543–546, Aug 2012.

[32] C. Bennett, P. Shor, J. Smolin, and A. Thapliyal, "Entanglement-assisted classical capacity of noisy quantum channels," *Physical Review Lettes*, vol. 83, pp. 3081–3084, Oct. 11 1999.

[33] C. E. Shannon, "A mathematical theory of communication," *Bell System Technical Journal*, vol. 27, pp. 379–423 and 623–656, June and Oct. 1948.

[34] P. Elias, "Coding for noisy channels," *IRE Conv. Rec. pt.4*, pp. 37–47, 1955.

[35] C. Berrou, A. Glavieux, and P. Thitimajshima, "Near Shannon limit error-correcting coding and decoding: Turbo-codes. 1," in *IEEE International Conference on Communications, 1993. ICC '93 Geneva. Technical Program, Conference Record*, vol. 2, pp. 1064 –1070 vol.2, May 1993.

[36] S. Lloyd, "Capacity of the noisy quantum channel," *Phys. Rev. A*, vol. 55, pp. 1613–1622, Mar 1997.

[37] P. W. Shor, "The quantum channel capacity and coherent information," *in Lecture Notes, MSRI Workshop on Quantum Computation*, 2002.

[38] I. Devetak, "The private classical capacity and quantum capacity of a quantum channel," *IEEE Transactions on Information Theory*, vol. 51, pp. 44–55, Jan 2005.

[39] B. Schumacher and M. D. Westmoreland, "Sending classical information via noisy quantum channels," *Phys. Rev. A*, vol. 56, pp. 131–138, Jul 1997.

[40] A. S. Holevo, "The capacity of the quantum channel with general signal states," *IEEE Transactions on Information Theory*, vol. 44, pp. 269–273, Jan 1998.

[41] H. F. Chau, "Quantum convolutional error-correcting codes," *Phys. Rev. A*, vol. 58, pp. 905–909, Aug 1998.

[42] M.Tücher and J. Hagenauer, "Exit charts of irregular codes," in *Proceeding of the 36th Annual Conference on Information Sciences and Systems [CDROM], (Princeton, NJ, USA)*, March 2002.

[43] H. Ollivier and J.-P. Tillich, "Description of a Quantum Convolutional Code," *Phys. Rev. Lett.*, vol. 91, p. 177902, Oct 2003.

[44] A. Ashikhmin, G. Kramer, and S. ten Brink, "Extrinsic information transfer functions: model and erasure channel properties," *IEEE Transactions on Information Theory*, vol. 50, pp. 2657–2673, Nov. 2004.

[45] I. Devetak and W. P. Shor, "The capacity of a quantum channel for simultaneous transmission of classical and quantum information," *Communications in Mathematical Physics*, vol. 256, no. 2, pp. 287–303, 2005.

[46] D. Poulin, J. P. Tillich, and H. Ollivier, "Quantum serial turbo-codes," in *2008 IEEE International Symposium on Information Theory*, pp. 310–314, July 2008.

[47] M. H. Hsieh and M. M. Wilde, "Entanglement-assisted communication of classical and quantum information," *IEEE Transactions on Information Theory*, vol. 56, pp. 4682–4704, Sept 2010.

[48] M. M. Wilde and M. H. Hsieh, "Entanglement boosts quantum turbo codes," in *Information Theory Proceedings (ISIT), 2011 IEEE International Symposium on*, pp. 445–449, July 2011.

[49] Z. Babar, S. X. Ng, and L. Hanzo, "Near-capacity code design for entanglement-assisted classical communication over quantum depolarizing channels," *IEEE Transactions on Communications*, vol. 61, pp. 4801–4807, December 2013.

[50] C.-Y. Lai, T. A. Brun, and M. M. Wilde, "Dualities and identities for entanglement-assisted quantum codes," *Quantum Information Processing*, vol. 13, no. 4, pp. 957–990, 2014.

[51] P. K. Sarvepalli, A. Klappenecker, and M. Rötteler, "Asymmetric quantum codes: constructions, bounds and performance," *Proceedings of the Royal Society of London A: Mathematical, Physical and Engineering Sciences*, vol. 465, no. 2105, pp. 1645–1672, 2009.

[52] P. Williams, H. Clearwater, *Ultimate Zero and One Computing at the Quantum Frontier*. New York, USA : COPERNICUS Springer-Verlag New York, 2000.

[53] M. A. Nielsen and I. L. Chuang, *Quantum Computation and Quantum Information*. Cambridge University Press, 2010.

[54] S. ten Brink, "Convergence behavior of iteratively decoded parallel concatenated codes," *IEEE Trans. Commun.*, vol. 49, pp. 1727–1737, Oct. 2001.

[55] L. Hanzo, T. H. Liew and B. L. Yeap, R. Y. S. Tee and S. X. Ng, *Turbo Coding, Turbo Equalisation and Space Time Coding: EXIT-Chart-Aided Near-Capacity Designs for Wireless Channels*. 2nd Edition New York, USA: John Wiley IEEE Press, March 2011.

[56] M. Tuchler, "Design of serially concatenated systems depending on the block length," *IEEE Transactions on Communications*, vol. 52, pp. 209–218, Feb. 2004.

[57] M. Tüchler, "Design of serially concatenated systems depending on the block length," *IEEE Transactions on Communications*, vol. 52, pp. 209–218, February 2004.

[58] H. V. Nguyen, C. Xu, S. X. Ng, and L. Hanzo, "Near-capacity wireless system design principles," *IEEE Communications Surveys and Tutorials*, vol. 17, pp. 1806–1833, Fourthquarter 2015.

[59] A. Ashikhmin, G. Kramer, and S. ten Brink, "Code rate and the area under extrinsic information transfer curves," in *Proc. IEEE International Symposium on Information Theory*, p. 115, 2002.